Metrol. Meas. Syst., Vol. XIX (2012), No. 2, pp. 231-244.

PAN POLSKA AKADEMIA NAUK

METROLOGY AND MEASUREMENT SYSTEMS

Index 330930, ISSN 0860-8229

www.metrology.pg.gda.pl

M&MS

ASSESSMENT OF CARDIOVASCULAR RISK IN ASSISTED LIVING

Jerzy Wtorek, Adam Bujnowski, Jacek Rumiński, Artur Poliński, Mariusz Kaczmarek, Antoni Nowakowski

Gdańsk University of Technology, Faculty of Electronics, Telecommunications and Informatics, Department of Biomedical Engineering, Narutowicza 11/12, 80-233 Gdansk, Poland (✉ jaolel@biomed.eti.pg.gda.pl)

Abstract

Disorders of the heart and blood vessels are the leading cause of health problems and death. Early detection of them is extremely valuable as it can prevent serious incidents (e.g. heart attack, stroke) and associated complications. This requires extending the typical mobile monitoring methods (e.g. Holter ECG, tele-ECG) by introduction of integrated, multiparametric solutions for continuous monitoring of the cardiovascular system.
In this paper we propose the wearable system that integrates measurements of cardiac data with actual estimation of the cardiovascular risk level. It consists of two wirelessly connected devices, one designed in the form of a necklace, the another one in the form of a bracelet (wrist watch). These devices enable continuous measurement of electrocardiographic, plethysmographic (impedance-based and optical-based) and accelerometric signals. Collected signals and calculated parameters indicate the electrical and mechanical state of the heart and are processed to estimate a risk level. Depending on the risk level an appropriate alert is triggered and transmitted to predefined users (e.g. emergency departments, the family doctor, etc.).

Keywords: wearable systems, cardiovascular risk, body sensor network

1. Introduction

Disorders of the heart and blood vessels are the leading cause of health problems and death. Cardiovascular complications increase with age. In the USA, approximately nine hundred thousand people die every year of complications from cardiovascular diseases, representing 38% of the overall mortality in this country [1]. In the industrialized world, mortality caused by cardiovascular diseases causes 16.7 million cases annually. Therefore, early detection of physiological changes is extremely valuable as it can prevent more serious symptoms (e.g. heart attack, stroke) and associated complications. This requires extending the typical mobile monitoring methods (e.g. Holter ECG, tele-ECG) by introducing integrated, multiparametric solutions for continuous monitoring of the cardiovascular system [2].

There have been many attempts to assess the state of the heart or blood vessels at home. Recently, a relatively sophisticated approach was proposed by Yan and co-workers [3]. A low power high resolution Thoracic Impedance Variance (TIV) device and a electrocardiographic (ECG) monitoring System on a Chip (SoC) package was developed and incorporated into a compact housing for wearable low-cost cardiac healthcare. Other approaches are less complicated as they deal with a particular activity or signal, e.g. blood pressure or ECG.

Of particular interest, is a non-invasive and continuous blood pressure measurement [4]. These attempts so far most rely on measurements of the transit time between two selected points of the cardiovascular system [5, 6].

It seems that measurement of a patient's ECG is the most popular solution and devices for personal measurement are already widely available on the market [7]. However, these type of devices are not suitable for complex monitoring purposes. The problem of continuous,

Article history: received on Feb. 3, 2012; accepted on Apr. 24, 2012; available online on May 18, 2012; DOI: 10.2478/v10178-012-0020-0.

complex monitoring of the cardiovascular system is still an open issue [8, 9]. The heart, or more generally, the cardiovascular system is a complicated one and needs simultaneous monitoring of the electrical, mechanical and biochemical conditions.

The heart consists of two pumps working in series and each consists of two chambers. Anatomically they are divided into the right and left heart. However, there is only one system of volume-pressure regulation. It is a biochemically powered and electrically activated organ. An action potential (AP) is generated, in the physiological state, by the sinoatrial node (Fig. 1). This pacing impulse propagates through the atria causing their contraction. The atria and ventricles are electrically isolated, i.e. propagation of AP is not possible between atria and ventricles. However, there is a small path electrically connecting the right atrium and intraventricular septum. The AP propagates through it and it does reach the ventricles. This phenomenon is observed on a thorax as ECG.

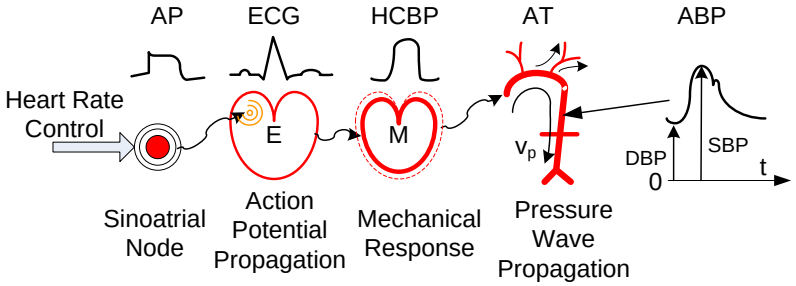

Fig. 1. A schematic presentation of the cardiovascular system, considered in this paper, AP – action potential, ECG – electrocardiogram, HCBP – heart chambers blood pressure, AT – arterial tree, v_p – velocity of propagation, ABP – artery blood pressure, DSB – diastolic blood pressure, SBP – systolic blood pressure.

The ventricles contract in response to the propagated AP and the blood pressure rises in both ventricles and blood starts to flow into the aorta (AT). The aorta accumulates in-flowing blood due to its expansion. At the same time the pressure pulse starts to propagate, with velocity v_p, through the arterial network down to small arterioles. The venous system and its associated blood flow are omitted here, as they are not considered in this paper.

A failure of the cardiovascular system may result in a serious threat to life. It may appear in a different part of the cardiovascular system and it may manifest itself in a different way. Furthermore, an appropriate medical response should be taken immediately after recognizing the disorder or susceptibility to a condition.

In this paper we propose a wearable system that integrates measurements of functional, hemodynamic data with actual estimation of the cardiovascular risk level. It consists of two devices, one designed in the form of a necklace, while the other is in the form of a bracelet (wrist watch). These devices enable continuous measurement of electrocardiographic, plethysmographic (impedance and optical) and accelerometric signals. They communicate between themselves and the necklace device also serves as the node of a wireless network.

2. Methods

In the following subsections a brief description of the developed system and its part are discussed more deeply. Basic information on the theoretical backgrounds of the method utilized, the hardware developed and the data processing methods used, are presented below.

2.1. The system

The system for evaluating cardiovascular parameters is built in the form of a central station/smartphone and a network of sensors (Fig. 2a). Other methods and approaches are exploited to gain information on the person's cardiovascular state, e.g. intelligent balance,

blood pressure meter (cuff method), glucometer, pulsoximeter (saturometer), and other also supply very useful information, however not as frequently as a wearable body sensor network (BSN). An appropriate combination of information obtained from different sources enables a more detailed picture of the monitored person to be formed. It should be underlined that the presented system is different from the seemingly similar one described as a Holter recorder.

The method of assessing selected parameters of the cardiovascular system's state, which are considered in this paper, are limited to the BSN which a small, but essential part of a more sophisticated system (Fig. 2a).

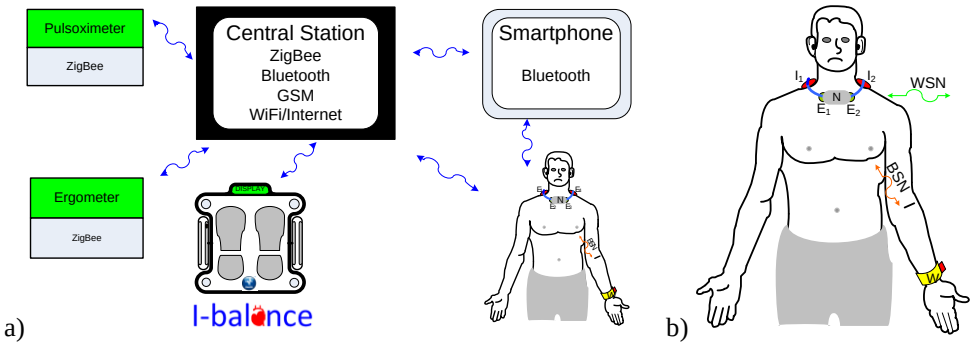

Fig. 2. A schematic presentation of the monitoring system, BP – blood pressure meter, a), and b) body sensor network, N – upper chest-neck node, W – wrist node, I_1, I_2, E_1, E_2 electrodes, BSN – body sensor network consisting of two sensors, WSN – communication between system and BSN.

The body sensor network consists of two sensor nodes devoted to non-invasive information collection from the human body on the cardiovascular system's state. One sensor node (the master) is placed on the neck (upper chest) while another (the slave) is placed on the patient's wrist (Fig. 2b). The neck-sensor enables recording of the following signals: an electrocardiographic signal (one lead), the impedance change of the thorax (i.e. the blood volume changes or movements and respiration activity), and body movements using a 3D accelerometer. The wrist-sensor enables recording of a photopletysmogram, hand movement (using an accelerometer) and a pressure reading using the sensor attachment to the wrist. The localization of the nodes is chosen to ensure reliable measurements and minimum discomfort for the assisted person (e.g. by hiding the sensors from the public view).

2.2. Theoretical principles of utilized measurement methods

As originally developed, in spite of using some already known methods and algorithms in the developed system, these are used in nonstandard manner and they therefore need a theoretical examination.

2.2.1. Spatial sensitivity for electrical potential measurement

Different leads utilized in standard electrocardiography are sensitive to peculiar part of the heart muscle. Therefore, it is impossible to monitor processes in the whole heart using a single lead. However, it is possible to evaluate the heart rhythm and of course, processes in the region of the heart to which this lead is the most sensitive. A voltage measured between electrodes forming the lead can be calculated using the following relationship [10]:

$$V_{LE} = \frac{1}{I_{LE}} \int \frac{1}{\sigma(x,y,z)} \mathbf{J}_{LE} \cdot \mathbf{J}^i dv \,, \tag{1}$$

where: $\mathbf{J}^i$ - is the local electrical activity of the heart (the so called impressed current flowing through a cell membrane), $\mathbf{J}_{LE}$ - the lead field determined by the electrode's shape,

configuration and placement, σ - the spatial distribution of conductivity. The unit current I_{LE} is a hypothetical one and it flows between electrodes forming the lead.

According to (1) the ratio $S_{EC} = \mathbf{J}_{LE}/\sigma(x,y,z)$, was used as the sensitivity of the lead to electrical activity of the heart for the developed configuration of the electrodes. A realistic model of the thorax, based on CT data obtained from an examination of a 68-year-old man was developed using image processing methods [11]. A finite element model including the lungs, heart, thorax wall, liver, skeleton and other anatomical organs consisted of 212 000 tetrahedral elements (more details in [12]).

2.2.2. Spatial sensitivity for electrical impedance measurement

To follow the phenomena associated with blood flow (movement) in the upper part of a thorax an impedance technique is utilized. Similar to the electrocardiographic method, a recorded signal is strongly dependent on the geometry of an object and electrode matrix configuration [13-15]. As a result, a similar relationship can be utilized to calculate the spatial distribution of the sensitivity. Assuming a four-electrode technique, the measured change of impedance for a given electrode configuration, geometry of the object, and spatial distribution of conductivity is described by the following relationship [16]:

$$\Delta Z = -\int_{v} \Delta\sigma(x,y,z)\frac{\nabla\phi(\sigma)}{I_{\phi}}\cdot\frac{\nabla\varphi(\sigma+\Delta\sigma)}{I_{\varphi}}dv, \tag{2}$$

where: $\sigma(x,y,z)$ - is the spatial conductivity distribution in the object, ϕ is the potential distribution associated with current I_{ϕ} between current electrodes while φ is the potential distribution associated with current I_{φ} (hypothetical) between voltage electrodes however, after conductivity change, $\Delta\sigma$ has appeared.

Therefore, a scalar product, $S_{TI} = \mathbf{L}_{\phi}\cdot\mathbf{L}^{t}_{\varphi}$, where $\mathbf{L}_{\psi} = \nabla\phi/I_{\phi}$ and $\mathbf{L}^{t}_{\phi} = \nabla\varphi/I_{\varphi}$, could be utilized as the sensitivity of a given electrode configuration to conductivity changes in the thorax. The same model of the thorax, presented in the previous subsection, was used to calculate the spatial distribution of the sensitivity of the impedance measurement technique.

2.2.3. Spatial sensitivity for photoplethysmographic measurements

The photoplethysmographic signal reflects blood perfusion in a tissue. Since the change in blood volume in the tissue is synchronous with heart contraction, it may be used for estimation of the propagation processes. A theoretical description of the photoplethysmographic signal belongs to the so-called forward problem of optical measurements. It means that a distribution of light intensity on an object's border is sought assuming that the light source placement and material properties are known. Therefore, a change in the recorded signal due to a change of the absorption coefficient is given by the relationship [17, 18]:

$$\Delta I_{d} = -\int_{v} \Delta\mu_{a}(\mathbf{r})G(\mathbf{r},\mathbf{r}_{s})\cdot G(\mathbf{r},\mathbf{r}_{d}), \tag{3}$$

where: ΔI_{d} - is the change of signal recorded by the detector, $\Delta\mu_{a}$ - is the change of the absorption coefficient, $G(r,r)$ - is the Green function for the diffusion equation, and correspondingly for the light source and photodetector. Thus, the integrand in the relationship (3) allowed the calculation of the developed optical sensor's sensitivity and its dependence on sensor's construction, assuming given properties of tissue.

2.3. Hardware

At the moment the wearable system consists of two nodes, however it would be easy to enlarge it with others. Nevertheless, it is assumed that the number of nodes should be as small as possible. It follows from the fact that an increase in the number of nodes involves a disproportional rise of inconvenience for the person being monitored.

2.3.1. The neck node

The neck node is devoted to measuring signals associated with heart activity (Fig. 3a). In practice, there are two types of signals to be measured, electrical and mechanical. The electrical activity, ECG, is measured directly while the mechanical one is measured indirectly using the impedance method. Both methods have to fulfil special requirements [15, 19, 20].

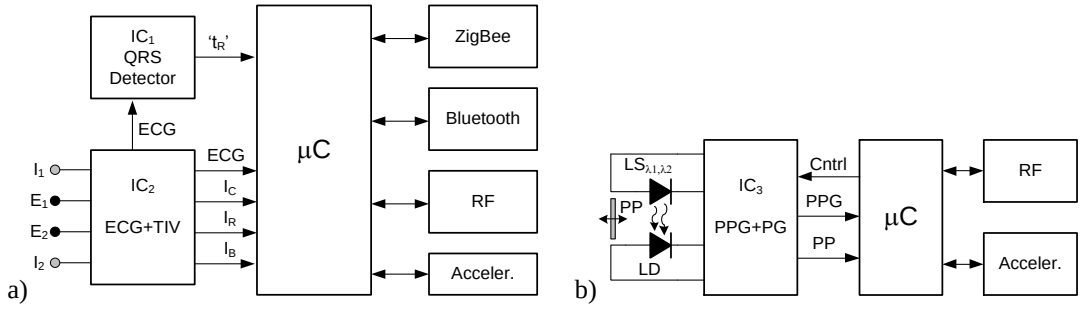

Fig. 3. a) A block diagram of the neck node, ECG+TIV - a circuit of electrocardiogram and impedance measurement, QRS Detector – a circuit for the detection of the QRS complex in the ECG, t_R – time marker indicating appearance of the QRS complex in the ECG, I_C, I_R, I_B – cardiac, lungs, basal components of TIV respectively, I_1, I_2, E_1, E_2 – current and voltage electrodes respectively, b) A block diagram of the wrist sensor node, PPG+PG photoplethysmogram and pressure measurement circuit, $LS_{\lambda1,\lambda2}$ - combined light source, LD – photodetector, Cntrl – control signal, PPG – photoplethysmogram, PP – pressure signal, RF – radio transceiver.

TIV, based on a four-electrode technique, is utilized for evaluation of mechanical phenomena associated with heart contraction and lung activity (more details on the circuitry can be found elsewhere, e.g. [21]). A custom developed and made integrated circuit, IC_2, enables simultaneous measurement of both signals using the same set of electrodes, I_1, I_2 and E_1, E_2. The ECG signal is sent to the microcontroller and to another circuit, developed in our laboratory, the hardware QRS detector. This circuit detects the QRS complex without any delay, during the time that the QRS complex continues to occur. Therefore, it can be utilized for the synchronization of the processing algorithm in both the wrist and neck nodes. Oversampling and decimation methods are applied when processing ECG and impedance signals (I_C, I_R, and I_B). Accelerometer (3D) is used for estimation of a person's body position (standing or lying). Bluetooth and ZigBee interfaces are used for communication in WSN while the RF (ISM 868 MHz) transceiver in BSN.

2.3.2. The wrist node

In comparison to the neck node, the wrist one is less complicated (Fig. 3b). It enables measurement of a photoplethysmogram, accelerations (3D), and pressure between the body of the sensor and the underlying tissue.

The photoplethysmogram is measured using a classical approach utilizing a LED - photodiode sensor. A special geometrical construction of the sensor has been developed to achieve a relatively small sensitivity to sensor displacement in relation to the radial artery.

The neck node detects the QRS complex and wirelessly (RF ISM 868 MHz) triggers the wrist node. In response, the wrist node transmits information containing status of the analysed signals and the calculated parameters of these signals. The neck node creates the measurement vector and sends it to the central station (ZigBee) or to the smartphone (Bluetooth).

2.4. Data processing

Data processing is distributed between measurement nodes and the decision module (the central station). Processing is limited in measurement nodes to reduce power consumption.

2.4.1. Signal preprocessing

Before parameterization of the signals is performed, they are pre-processed. In order to reduce the complexity of the circuitry oversampling is used and then decimation techniques are utilized. The measured signals are filtered according to demands specified for each signal.

2.4.2. Parameterization of signals

Both parameters are calculated for single signals as well as those describing relations between them. Based on the ECG, the heart rate (HR), and width of the QRS complex, T_{QRS}, are determined. The TIV signal is used to determine the rise time of the impedance change associated with the ventricle contraction, $T_{r\Delta Z}$, the rise time of impedance change rate, T_{rdZ}, and amplitude of impedance change caused by the ventricles contraction, $A_{\Delta Z}$. In turn, the PPG signal recorded in the wrist node is analyzed in order to assess its amplitude, A_{PPG}, rise time, T_{rPPG}, and maximal rate dPG_m. The modulus of both accelerometric signals (from the neck and wrist nodes) each consisting of three components, is also determined, A_{ccn} and A_{ccw}.

Next, the following parameters describing the relationship between signals are calculated: time delay between the R wave in ECG and the beginning of impedance ejection wave, $T_{R\text{-}E}$, time delay between the beginning of ejection wave and plethysmographic one, $T_{E\text{-}P}$.

The specified parameters allow classification of the excitation type (normal, arrhythmic, atrial fibrillation, etc), estimation of heart contractility (HI_m – modified Heather Index, HC_f – cardiac contractility variation related to heart rate variation, $HC_{V\text{-}M}$ – heart isovolumetric contraction time to maximum rate of contraction time ratio), continuous evaluation of the blood pressure (based on the understanding of TIV and PPG signal amplitudes, $A_{v\Delta Z}$, and A_{PPG}, and time delay, $T_{E\text{-}P}$), and physical activity of the person (accelerometric signals are utilized).

The result of parameterization of the signals leads to a measurement vector:

$$\{..., HR, T_{QRS}, T_{r\Delta Z}, T_{rdZ}, A_{\Delta Z}, A_{PPG}, T_{rPPG}, dPG_m, A_{ccn}, A_{ccw}, T_{R\text{-}E}, T_{E\text{-}P}, HI_m, HC_f, HC_{V\text{-}M}, ...\}$$

In fact, the vector of parameters is larger as it contains other parameters not discussed here, e.g. respiration rate and status of analyzed signals, e.g. level of noise. It can be further enlarged by introduction of other indicators derived from the measured signals. The measurement vector constitutes the input for the decision module.

2.4.3. Risk assessment

The developed wearable system for the evaluation of the state of the cardiovascular system needs to communicate with a node responsible for the processing of vectors of parameters and for further actions, e.g. triggering an emergency alert. This node can be the central, computer station (in a home environment, using ZigBee) or a smartphone (when outside home, using

Bluetooth). A dedicated software has been developed to enable wireless communication, and synchronization between the wearable system, the smartphone, and the central station. The common function of the central station and the smartphone is to classify the vectors of the parameters and perform further actions, including transmission of alerts to predefined recipients. However, the software on the central station can use additional parameters for classification and decision making collected by other sensors used at home. Also parameters of long-term trend analysis can be used. In this paper we focused on measurement methods used by the wearable system, so the software component and classification analysis is presented here only to illustrate the overall goal of our research.

A block diagram of the decision taking module is presented in Fig. 4. First, the level of noise (e.g. outliers) in data is estimated to perform a data-cleaning operation. All parameters are stored, however, only those satisfying the predefined criteria are used for further processing.

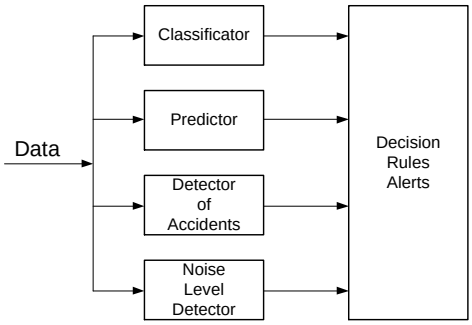

Fig. 4. A block diagram of the decision module.

For example, if there is a large break in receiving of some measurement data or there is an unacceptable level of noise for a longer period, an appropriate alert is generated (e.g. ECG data too noisy, communication problem between nodes of the wearable system, etc.). A time stamp marks all alerts. After the data cleaning operation three parallel operations are performed for the measurement vector: detection of accidents, data classification, and prediction.

Detection of accidents is used for discovering unusual personal behavior (e.g. using activity measurements with accelerometers) and for recognizing a risk related to an individual parameter from the measurement vector (e.g. irregular, increased heart rate). In the home environment the number of possible accidents is higher, since additional parameters are available for analysis (e.g. from the intelligent scale sensor, from the glucometer, etc.). Detection of accidents is based on predefined thresholds chosen for a given, assisted person and tuned to his/her activity model (e.g. different criteria for a day and night). The chosen thresholds can be adaptively modified through the learning procedure. This requires some history of previous observations (measured parameters and accidents classified into true positive/negative and false positive/negative). In some situations individual parameters are within a normal, acceptable range for a given person, while a combination of them indicates an unusual state, dangerous situation, or can be an indicator of the incoming complication (e.g. the delay in the electromechanical coupling of the heart) [22]. The multiparameter classification can be used to detect such situations. The predictor in the decision module allows including the model of the monitored person (based on the prior observations) in classification and can be used as a source of alerts when a significant deviation of measured data from the predicted ones is observed. This is especially important since a fast response of caregivers is mostly required for cardiovascular problems. The decision module maps the results of the parameter evaluation blocks (detector of accidents, classifier, predictor) into alerts. The alert types and associated recipients are presented in Table 1.

Table 1. The mutual relationship between the types of alerts and typical actors of the support system.

Alert priority/alert recipient	Emergency teams	GP/ Personal doctor	Nurse/social service	Relatives/ guardians	Neighbours	Assisted person
0 (emergency)	X	X	X	X	X	X
1 (alarm)		X	X	X	X	X
2 (warning)			X	X		X
3 (system error)				X		X
4 (serious problem)			X	X	X	X
5 (problem)						X

Further discussion related to the alerts of the developed system is presented in [2].

3. Results

The relationships (1-3) have been used for selecting the best configuration of the electrode matrix (electrical and impedance measurements) and the probe construction (optical sensing). Simulations were performed using the Finite Element Method [12, 14]. Exemplary results for each type of the sensitivity are presented in Figs 5 and 6a.

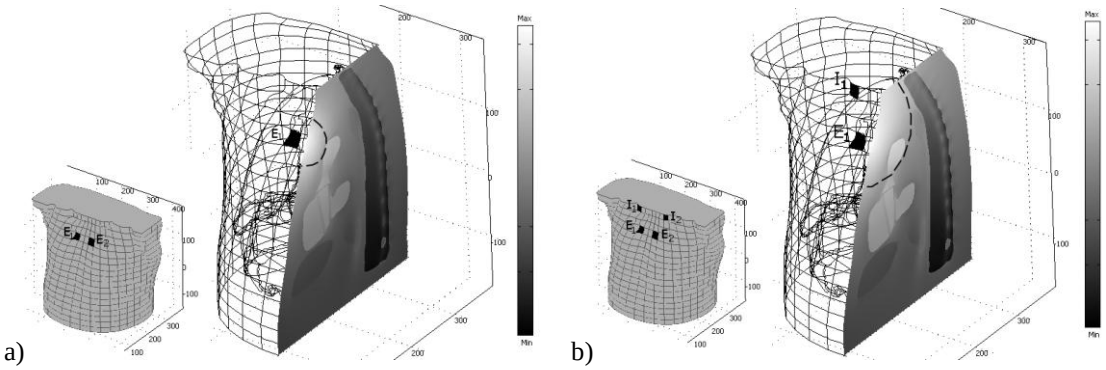

Fig. 5. Distribution of the sensitivity (arbitrary units) for electric potential a) and for impedance measurement b) assuming given electrode placement (E_1, E_2 or I_1, I_2, E_1, E_2), the thorax shape, and spatial conductivity distribution. Modulus of the sensitivity is presented for potential measurement. Only the sensitivity on the sagittal plane is presented. The dashed line indicates a drop of the sensitivity by 20% from the highest value marked white.

The sensitivity of the measurement method to the localization of electrical dipoles in the thorax was calculated for different conductivity distributions in the thorax. An example of the results obtained is presented in Fig. 5a. As expected, according to its definition, the highest values were located close to electrodes. However, the source of the measured electrogram was located in the myocardium. Therefore, the total sensitivity was calculated separately for the atria $S_{ca} = (0.38 \div 0.55)$ Vm^2, and ventricles, $S_{cv} = (0.45 \div 0.62)$ Vm^2.

The sensitivity of the electrode matrix to the conductivity changes in the chest (Fig. 5b) was similar to the sensitivity for measurement of electric potentials. The impedance method was sensitive to the conductivity changes observed in the chest. Contributions from the aorta, atria, ventricles, and lungs were correspondingly $S_{ia} = (0.4 \div 0.6)$ Ωm^2, $S_{im} = (0.01 \div 0.04)$ Ωm^2, $S_{iv} = (0.01 \div 0.03)$ Ωm^2, and $S_{il} = (0.2 \div 0.28)$ Ωm^2. It was calculated assuming $\Delta\sigma = 0$. The changes of conductivity, among others, may arise from blood displacement in the chest, which is characterized by the heart like dynamics. The Δz wave associated with ventricle contraction or aortic volume change is the most valuable in the considered application. It allows to determine a time point of the aortic valve opening and dynamics of the heart contraction.

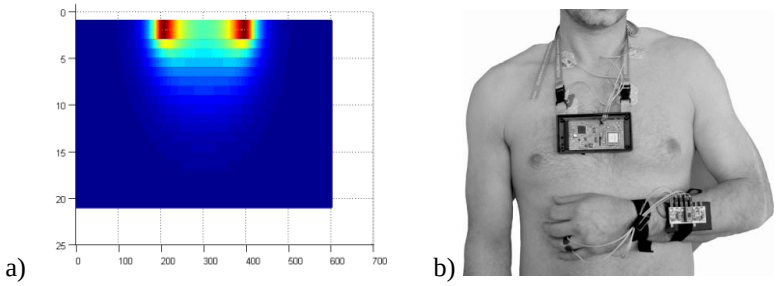

Fig. 6. a) Distribution of the sensitivity for optical measurements (green light), values on plane perpendicular to the tissue and containing source and detector are shown. b) The working prototype of the wearable system.

Spatial sensitivity for the optical measurements was calculated for a simplified tissue model (Fig. 6a). The tissue model was uniform and semi-infinite with the surface described by the plane $z = 0$. The penetration depth of the light depended on the wavelength. The following characteristic depth values were obtained: 0.8 mm for the red light, 0.5 mm for the green light, and 0.3 mm for the blue light.

Noise levels were measured for the neck node. Standard deviation of noise related to the output was 1.4 mΩ and 2.8 mV, respectively for the TIV and the ECG measurements. Next, the measurements using the prototype of the wearable system (Fig. 6b) were performed.

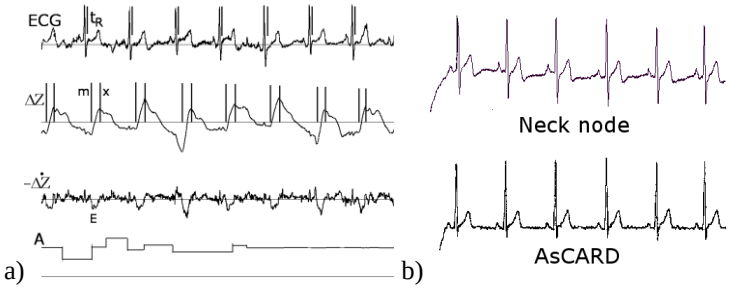

Fig. 7. Signals recorded using the neck node a) and ECG recorded simultaneously using the neck node and the AsCARD b), ECG – electrocardiogram, ΔZ - change of impedance, $\Delta\dot{Z}$ - rate of impedance change, A - modulus of signals from the three-axial accelerometer, t_R - impulse generated by the detector of the QRS complex, m -indicator of beginning of the ejection wave, x - indicator of ΔZ wave maximum , E -ejection wave.

Eight healthy volunteers (av. age: 42 ± 5, 6 males, 2 females) took part in experiments (examples of the recorded signals are shown in Figs. 7 and 8).

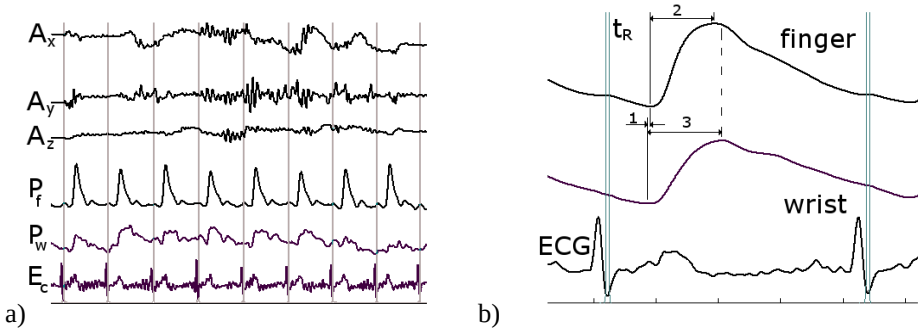

Fig. 8. Signals recorded using the wrist node a) and enlarged version of PPG signals b), A_z, A_y, A_x components of the accelerometric signal, P_f – photoplethysmogram measured on a finger, P_w – photoplethysmogram measured on the wrist, t_R – reference signal indicating the position of the QRS complex, "1" time delay between PPG registered at the wrist and finger, "2","3" – rise time of finger's and wrist's signals respectively.

Validation of electrocardiographic measurements by the neck node was performed using the AsCARD electrocardiograph (Fig. 7b) (lead I, AsCARD MrGrey v.201, Aspel) [23]. In

Fig. 8a examples of signals from the wrist node are presented. The signals were recorded for hand kept moving on a table surface with spontaneous finger tapping. An enlarged version of signals (Fig. 8b) shows more detailed relationships between them. Results of all measured and calculated parameters are collected in the form of measurement vectors and sent to the central station at each heart beat (QRS detection) (Table 2).

Table 2. Examples of measurement vector data.

...	HR	T_{QRS}	$T_{r\Delta Z}$	T_{rdZ}	$A_{\Delta Z}$	A_{PPG}	T_{rPPG}	dPG_m	A_{ccn}	A_{ccw}	T_{RE}	T_{EP}	HI_m	HC_f	HC_V
	bpm	ms	ms	ms	mΩ	a.u.	ms	a.u./s	m/s²	m/s²	ms	ms	Ω/s²	Ω	1
i	71	75	130	32	65	550	60	11.2k	0.0	0.0	200	60	15.6	0.14	0.25
i+1	73	73	136	40	67	580	55	12.9k	0.0	0.3	205	66	12.4	-0.17	0.29
i+2	70	73	128	39	62	600	58	12.0k	0.0	0.4	199	62	12.4	0.03	0.31

Detection of accidents was tested using data collected for patients with disorders of the cardiovascular system, recorded at the Intensive Care Unit. In Fig. 9 examples of the variability of recorded parameters are presented (68 years male, HR=123.8±14.92; SBP=116.53±21.05; DBP=47.93±8.7.

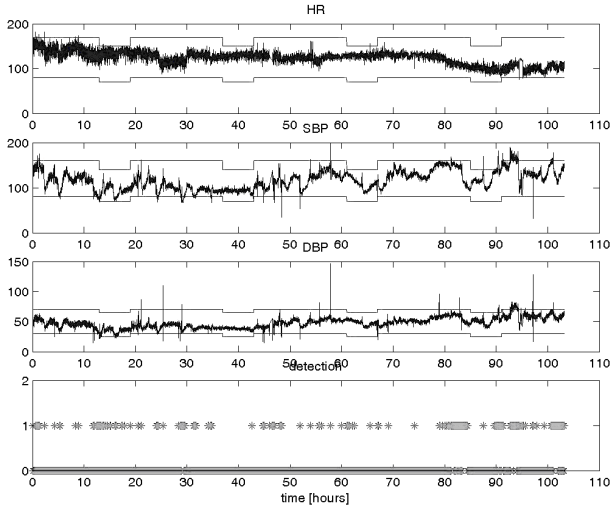

Fig. 9. Detection of accidents using fixed thresholds for the values of the heart rate and the systolic/diastolic blood pressure. Accidents are indicated using value "1" on the lowest chart.

Additionally, the results of the detection of accidents using fixed thresholds are shown. There are different thresholds levels for a day (6:00 – 24.00) and night (0:00-6:00). The decision module further processes the detected accidents making a decision about possible alert (and its priority).

4. Discussion

Development of wearable, mobile systems for assisting chronically ill or old people is very important for the aging society [24]. Proposals presented in the literature and available on the market are mainly focused on a selected physiological activity. Currently, most of the proposals and ongoing research related to the topic considered in the paper are in the developing stage, both hardware and software (e.g. [3, 8, 9]).

In this paper the wearable system for integrated measurement of the cardiovascular system parameters is described. The main attention is focused on measurements methods and their reliability and validity. The proposed methods rely on simultaneous evaluation of the electrical and mechanical performance of the heart and on the electromechanical coupling. Such approach is especially important for persons with chronicle heart failure or high risk of stroke [22].

It should be underlined that even in a case of using widely known method, however in a nonstandard application, serious theoretical and experimental examinations of its properties were required and performed. The experimental evaluation of the sensitivity approach has been validated in this paper and previously in [25, 26]. Thus, the methods used and results obtained can be considered as reliable. Moreover, the results obtained are reasonable and intuitively correct. The sensitivity to the electrical events in the chest is represented by a vector, the hypothetical current density weighted by the local conductivity. Therefore, for each point of the model, three components of the sensitivity should be presented. In the Results section only the modulus of the sensitivity is presented. Assuming that cells (myocytes) are cylindrical and, to some extent, uniformly oriented in different directions, the modulus of the sensitivity can be reasonably approximated. Furthermore, in spite of a great number of finite elements used in the model, their dimensions are much bigger than cellular ones. So, when assigning to each element a local activity (current density, $\mathbf{J}'$), such approximation is justified. The sensitivity of the electrode matrix used in the study to depolarization current flowing in the atria and ventricles is almost similar. It is a desired property of the method. Enhanced sensitivity to the atria makes the method more suitable for detection of atrial fibrillation.

The impedance method is widely used for estimation of blood flow induced mechanical events in the human body (e.g. [13, 26]). This method reflects, according to the relationship (2), all conductivity and volume changes undergoing in the space of nonzero sensitivity. Integrating the sensitivity over anatomical regions (i.e. aorta, atria, ventricles, etc.) allows the calculation of contribution from these regions to the measured signal. It follows from our examinations that the contribution from aorta dominates for the utilized electrode configuration. However, the relation between the contributions from the aorta to other regions may change interpersonally. It follows from the fact that the sensitivity and thus also the contribution from different regions (organs) depends on the conductivity of tissues and organs. These values are not fixed and each person is characterized by different set of conductivity values. It should be underlined that the sensitivity associated with a certain region/organ does not determine the value of the measured impedance change. The value of conductivity change, $\Delta\sigma$, and its spatial volume are other important factors (see (2)). The derivative of the impedance signal $\Delta\dot{Z}$ resembles blood ejection from the left ventricle (e.g. compare with [27]). Thus, the spatial distribution of the sensitivity is appropriate for detecting the conductivity changes arising from the aorta. However, further experimental studies are needed to prove it.

The distribution of the sensitivity for optical measurements showed a dependence on wavelength of the light. We used a very simple model to calculate the Green functions and the resulting sensitivity. The obtained distributions and values of depth penetration were in agreement with those published elsewhere (e.g. [28, 29]). However, because of the simplicity of the model used, they can be considered only as qualitative ones. Nevertheless, it follows from the performed examinations that different sources of light should be used for transmittance and reflectance sensors. It is not shown in the paper and thus not discussed in detail that the optical measurements are relatively strongly corrupted by hand movements.

The neck node allows measurement of the ECG, the impedance change and accelerometric signals. The quality of recorded signals is satisfactory as it is shown in Figs. 7 and 8, in spite

of electrode phenomena [20]. It is possible to automatically recognize and detect characteristic points of the signals which are essential in further processing. For comparison, the ECG was registered using the developed node and the commercial system. The recorded impedance signal, ΔZ, enables determining a time point when the aortic valve opens. Therefore, it is possible to determine the transition time of pulse pressure between the heart and a selected point of the circulatory system (e.g. the wrist). This in turn may be used for non-invasive blood pressure estimation or at least its changes.

A reflectance and transmittance sensors were developed for this purpose (the wrist node). PPG can be recorded simultaneously at the wrist and at the finger (arbitrary one) (Fig. 8a). The latter signal is, at the moment, used for achieving a more precise determination of the beginning PPG measured at the wrist. There is a difference between the signal measured at the wrist and at the finger (Fig. 8b). The PPG at the wrist was measured with the smallest force of sensor's attachment to the skin. This force essentially influences the shape of the recorded signal. It is due to the "wall load" effect. On the other hand, it is also an indirect evidence that the source of the signal is a radial artery. Furthermore, it appears a little in advance and is characterized by longer rise time than that of the signal recorded at the finger (Fig. 8b). In fact, it is easier to record PPG at the finger than at the wrist. However, the source of the signal is different in these two cases. In the former one the signal arises from small arteries while in the latter from the big vessel. It is important, when considering these measurements for estimating blood pressure.

In this work, estimation of the blood pressure changes was based on the pulse transit time technique [6]. Estimation of this time was made possible using RF communication between the neck and wrist nodes. At the time of QRS detection an RF signal was sent to the wrist node. The RF signal, aside from triggering an algorithm of the PPG signal analysis, was treated as a reference time by the wrist node.

The neck node is powered by a battery (MinMax LP604977 LiPo cell) of 2400 mAh capacity. It consumes less than 80 mA in the operating mode without active communication (ZigBee/Bluetooth). It increases to 140 mA, when the node continuously transmits data packets. During the experiment, the nodes were operating in the monitoring mode. In this mode, a set of parameters was transmitted for each detected QRS complex and additionally digital ECG/TIV signals were transmitted at the time of accident/anomaly detection. It was found that a single battery charge lasts for at least 24 hours of continuous work of the wearable system.

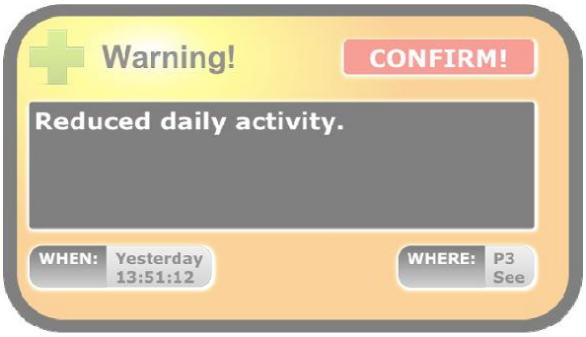

Fig. 10. A message sent by the system to the user and displayed on the TV set screen.

The properties and features presented above make the developed system very useful in monitoring persons with heart failure or, in general, suffering from insufficiency of the cardiovascular system. Its value is further increased by integrating it with the multimodal platform (Fig. 10), and in the result, by introducing an interactive schemes in decision-making procedures [2].

It has been shown that it is possible to design and implement the integrated, wearable system, which enables continuous measurements and parameterization of electrical and mechanical performance of the cardiovascular system and simultaneous activity of the assisted person. The parameter values obtained for the group of volunteers indicated full agreement with results measured using clinical, stationary systems. In this paper we focused on measurement aspects of the wearable system. Further research is required to evaluate and validate algorithms of the decision module for large data sets.

5. Conclusions

In this study we proposed a wearable system enabling the evaluation of electromechanical coupling of heart activity. Additionally, the system allows correlation of physical activity of the assisted person with the state of the cardiovascular system.

A set of parameters describing electrical and mechanical activity of the heart is measured for each heart contraction. Basing on these measurements the electromechanical coupling is also estimated. Moreover, the velocity of pulse pressure propagation is also determined. In the result, the cardiovascular system is integrally examined. This approach allows the continuous collection of essential information about the health status. It is an invaluable feature of the developed system, both for assisted persons, their relatives and physicians.

In home environment the measurements from the wearable system can be enriched with data from other sensors (e.g. intelligent scales, glucometers, etc.). There is also the very important, often not considered, advantage of long-term measurements at home. The trend analysis of long-term data can provide valuable indicators of health-related problems.

Additionally, the proposed system can reduce the cost of healthcare by early detection of health incidents. In an aging society it also offers an assistance that cannot be supported by limited human resources.

Acknowledgments

This work was partially supported by the European Regional Development Fund in frame of the project: UDA-POIG.01.03.01-22-139/09-02 -"Home assistance for elders and disabled – DOMESTIC", Innovative Economy 2007-2013, National Cohesion Strategy.

References

[1] *www.americaheart.org/statistics*, (2011).

[2] Kaczmarek, M., Rumiński, J., Bujnowski, A. (2011). Multimodal platform for continuous monitoring of elderly and disabled. *Proc. of the Federated Conference on Computer Science and Information Systems 2011, IEEE Xplore*, 393-400.

[3] Yan, L., Bae, J., Lee, S., Roh, T., Song, K., Yoo, H.-J.A. (2011). 3.9 mW 25-Electrode Reconfigured Sensor for Wearable Cardiac Monitoring System. *IEEE Journal of Solid-State Circuits*, 46(1), 353-364.

[4] Jung, J. H., et al. (2007). Estimation of the blood pressure using arterial pressure-volume model. In *Proceed. 6th International Special Topic Conference on ITAB*, Tokyo.

[5] Cox, R.H. (1968). Wave propagation through a Newtonian fluid contained within a thick-walled, viscoelastic tube. *Biophys J*., 8, 691-709.

[6] Marcinkevics, Z., Greve, M., Aivars, J.I., Erts, R., Zehtabi, A.H. (2009). Relationship between arterial pressure and pulse wave velocity using photoplethysmography during the post-exercise recovery period. *Acta Univesitatis Latviensis*: *Biology*, 753, 59-68.

[7] Omron (2012). Portable, cordless, single-channel ECG Monitor, Model HCG-801, *http://www.omron-healthcare.com/en/product/electro_cardiograph/HCG-801-E.html*.

[8] Oresko, J.J., et al. (2010). A Wearable smartphone-based platform for real-time cardiovascular disease detection via electrocardiogram processing. *IEEE Trans. on ITB*, 14(3), 734-740.

[9] Catherwood, P.A. (2010). ECG Motion Artefact Reduction Improvements of a Chest-based Wireless Patient Monitoring System. *Computing in Cardiology*, 37, 557-560.

[10] Malmivuo, J., Plonsey, R. (1995). Bioelectromagnetism – Principles and applications of bioelectric and biomagnetic fields. *Oxford Univ. Press*.

[11] Skalski A., Turcza P. (2011). Heart segmentation in echo images. *Metrol. Meas. Syst.*, 18(2), 305-314.

[12] Lewandowska, M., Wtorek, J., Bujnowski, A., Mierzejewski, L. (2010). Monitoring of CRT by means of impedance multiple measurements – simulation studies. *Journal of Physics: Conference Series*, 224, 012162.

[13] Wtorek, J. (2003). Impedance techniques in medicine. GUT Publishing Office. *Monographs Series*, 43, Gdansk, Poland.

[14] Wtorek, J., Poliński, A. (1995). Examination of impedance cardiography properties-FEM model studies. *Biomedical Sciences Instrumentation*, 31, 77-82.

[15] Wtorek J. (2003). Spatial sensitivity the conductivity changes of a four-electrode probe. *Metrol. Meas. Syst.*, 10(1), 3-16.

[16] Geselowitz, D.B. (1971). An application of electrocardiographic lead theory to impedance plethysmography. *IEEE Trans. Biomed. Eng.*, BME, 18(1), 38-41.

[17] Arridge, S.R., Hebden, J.C. (1997). Optical imaging in medicine: II. modelling and reconstruction. *Phys. Med. Biol.*, 42(5), 841-853.

[18] Trybuła, A. (2009). An application of diffusive optical tomography in functional examination of organs. *PhD Thesis*, Warsaw University of Technology. (in Polish)

[19] Santos, J., Ramos, P.M. (2011). DSPIC-based impedance measuring instrument. *Metrol. Meas. Syst.*, 18(2), 185-198.

[20] Tomczyk, K. (2011). Procedure for correction of the ECG signal error introduced by skin-electrode interface. *Metrol. Meas. Syst.*, 18(3), 461-470.

[21] Wtorek, J., et al. (2010). Simultaneous monitoring of heart performance and respiration activity. In *Proceed. of the 3rd IEEE Conference on HSI*, Rzeszów, Poland, 661-665.

[22] Badano, L.P., et al. (2007). Left ventricular electromechanical delay in patients with heart failure and normal QRS duration and in patients with right and left bundle branch block. *Europace*, 9, 41-47.

[23] AsCARD, producer home page: *http://www.aspel.com.pl*.

[24] Polak, A.G., et al. (2010). Telemedical system "Pulmotel-2010" for monitoring patients with chronic pulmonary diseases. *Metrol. Meas. Syst.*, 17(4), 537-548.

[25] Wtorek, J., Józefiak, L., Poliński, A., Siebert, J. (2002). An Averaging Two-Electrode Probe for Monitoring Changes in Myocardial Conductivity Evoked by Ischemia. *IEEE Trans. Biomed. Eng.*, 49(3), 240-246.

[26] Wtorek, J., Poliński, A. (2005). The contribution of blood-flow-induced conductivity changes to measured impedance. *IEEE Trans. on Biomed. Eng.*, 52, 41-49.

[27] Hahn, J.O., et al. (2005). Adaptive Left Ventricular Ejection Time Estimation Using Multiple Peripheral Pressure Waveforms. *Proceed. of the IEEE Eng. Med. Biol. 27th Ann. Conf. Shanghai*, China, 2383-2386.

[28] Okadai, E., Firbank, M., Delpy, D.T. (1995). The effect of overlying tissue on the spatial sensitivity profile of near-infrared spectroscopy. *Phys. Med. Biol.*, 40, 2093-2108.

[29] Huang, F.-H., et al. (2011). Analysis of reflectance photoplethysmograph sensors. *World Academy of Science, Engineering and Technology*, 59, 1266-1269.